

Structured Stochastic Quasi-Newton Methods for Large-Scale Optimization Problems

Minghan Yang*, Dong Xu†, Yongfeng Li‡, Zaiwen Wen§, Mengyun Chen¶

June 18, 2020

Abstract

In this paper, we consider large-scale finite-sum nonconvex problems arising from machine learning. Since the Hessian is often a summation of a relative cheap and accessible part and an expensive or even inaccessible part, a stochastic quasi-Newton matrix is constructed using partial Hessian information as much as possible. By further exploiting the low-rank structures based on the Nyström approximation, the computation of the quasi-Newton direction is affordable. To make full use of the gradient estimation, we also develop an extra-step strategy for this framework. Global convergence to stationary point in expectation and local suplinear convergence rate are established under some mild assumptions. Numerical experiments on logistic regression, deep autoencoder networks and deep learning problems show that the efficiency of our proposed method is at least comparable with the state-of-the-art methods.

1 Introduction

Consider the finite-sum optimization problem:

$$\min_{\theta \in \mathbb{R}^n} \Psi(\theta) = \frac{1}{N} \sum_{i=1}^N \psi_i(\theta), \quad (1)$$

where θ is the decision variable, ψ_i is a component function related to a given data point (x_i, y_i) and N is the number of data. Problem (1) widely arises in many applications such as deep learning [8, 33, 20, 30, 14, 10], statistic learning [13, 37], image processing [7] and etc.

A well-known method for (1) is the stochastic gradient descent method (SGD) [28]. There are many extensions by incorporating variance reduction techniques and acceleration schemes for practical improvements and theoretical guarantees [18, 24, 1]. In deep learning, stochastic first-order approaches [9, 35, 19, 12, 41] have been the first choice because of good generalization ability and the ease of implementation, etc.

Stochastic second-order methods have also gained much attention recently. Although the computation and inversion of the Hessian matrix in the large-scale applications is costly, various strategies to approximate the Hessian have been developed in [6, 29, 39, 27, 23, 40]. The key is to find an ingenious but cheap way to incorporate local curvature information. Particularly, stochastic quasi-Newton methods including the limited-memory BFGS (L-BFGS) are used to construct tractable approximations [32, 11, 5, 3, 38, 40]. In deep learning, stochastic second-order methods can also address the scalability issue with large batch sizes for the robustness with respect to hyperparameters.

*Beijing International Center for Mathematical Research, Peking University, China. E-mail: yangminghan@pku.edu.cn

†Beijing International Center for Mathematical Research, Peking University, China. E-mail: taroxd@pku.edu.cn

‡Beijing International Center for Mathematical Research, Peking University, China. E-mail: yongfengli@pku.edu.cn

§Beijing International Center for Mathematical Research, Peking University, China. E-mail: wenzw@pku.edu.cn

¶Huawei Technologies Co. Ltd, China. E-mail: chenmengyun1@huawei.com

The Hessian-free method [21] uses the conjugate-gradient (CG) method to obtain a descent direction by utilizing Hessian matrix-vector multiplications. The curvature information is estimated and added to SGD at each step in [15]. The Gauss-Newton matrix is investigated to approximate the Hessian matrix in [31]. A practical block-diagonal approximation to the Gauss-Newton matrix is studied in [4]. The so-called KFAC method developed in [22] takes advantage of the Fisher matrix and its block-diagonal approximation. Its efficiency has been demonstrated in large-scale distributed parallel computing [26].

The partial Hessian information has been taken in a few second-order methods. For example, the Gauss-Newton method for nonlinear least squares problems ignores the complicate part of the Hessian matrix and shows good performance on small residual problems. On the large residual problems, approaches that compensate the Gauss-Newton matrix by a quasi-Newton approximation to the complicate part of the Hessian matrix are often much better [25, 34]. This concept has been further verified in optimization problems with orthogonality constraints in [17]. In this paper, we exploit the partial Hessian information in the stochastic setting for problem (1).

Our main contribution are as follows.

- The structures where the Hessian matrix is a summation of a relative cheap and accessible part and an expensive or even inaccessible part are exploited for machine learning problems. Naturally, our strategy is to keep the cheap part but design a good approximation for the expensive part. When only a few samples are allowed, the Nyström approximation is helpful to construct a low-rank surrogate with certain theoretical guarantees.
- A general stochastic structured quasi-Newton framework is proposed for the large-scale non-convex finite-sum problem (1). We formulate a stochastic secant condition based on the partial Hessian matrix. Then, various quasi-Newton matrices can be computed. They usually provide better performance than these constructed by the vanilla quasi-Newton methods. We also develop an extra-step strategy to reuse the stochastic gradient estimated in the construction of the quasi-Newton matrix.
- Global convergence is established if the step sizes are chosen properly and the stochastic errors satisfy certain summability conditions. A local r-superlinear convergence rate is also proved for a general stochastic quasi-Newton method under a stochastic variant of Dennis-Moré condition.

The rest of the paper is organized as follows. The Hessian matrices are exploited with the Nyström approximation in Section 2. Our structured quasi-Newton method is developed in Section 3 and its theoretical properties are analyzed in Section 4. Numerical comparisons in Section 5 on the logistic regression, deep autoencoder networks and deep learning problems show that the performance of our proposed method is at least comparable with the state-of-the-art methods.

2 Structures of the Hessian Matrices

In this paper, we assume that the Hessian matrix $\nabla^2\Psi(\theta)$ can be divided into two different parts:

$$\nabla^2\Psi(\theta) = H(\theta) + \Pi(\theta), \quad (2)$$

where the part $H(\theta)$ is relatively cheap and accessible while the other part $\Pi(\theta)$ is expensive or even not computable. Specifically, there are a few possible reasons and strategies. i) The dimension n of θ is so large that an explicit storage of $\nabla^2\Psi(\theta)$ is prohibitive. Hence, it is favorable to use the Hessian information implicitly. ii) The derivatives are simply too complicate in certain cases. It is quite common that extensive evaluations of the partial Hessian matrix-vector multiplications are not feasible but executing a few of them carefully can be beneficial for the acceleration of the algorithms. There are certain limitations on the calculation of the Hessian information in deep learning due to some constraints imposed by the implementation of the data structures. iii) Even if each component $\nabla^2\psi_i(\theta)$ is cheap, assembling all components at each iteration becomes a non-negligible task when the size N in problem (1) is huge. Consequently, subsampling is ubiquitous in stochastic methods.

We next explain a few typical scenarios of (2). The goal is to explore $\Pi(\theta)$ for better performance at a relatively low computational cost.

2.1 Subsampling of the Hessian Matrices

The subsampling procedure only selects a small fraction of the data in certain ways for the update. Given a subset $\mathcal{S}_H \subseteq \{1, 2, \dots, N\}$, the subsampled Hessian matrix is defined as $\nabla_{\mathcal{S}_H}^2 \Psi(\theta) := \frac{1}{|\mathcal{S}_H|} \sum_{i \in \mathcal{S}_H} \nabla^2 \psi_i(\theta)$. It is common to choose the subset \mathcal{S}_H randomly with or without replacement. It can also be updated in a cyclical fashion or other suitable deterministic way. Note that shuffling or accessing the data randomly itself may be time-consuming due to the computer/memory architectures. The size $|\mathcal{S}_H|$ of the subset is an important factor for the behavior of the algorithms. If $|\mathcal{S}_H|$ is small, we can obtain easily

$$H(\theta) = \nabla_{\mathcal{S}_H}^2 \Psi(\theta). \quad (3)$$

However, it is not economic to use the matrix $\Pi(\theta) = \nabla^2 \Psi(\theta) - \nabla_{\mathcal{S}_H}^2 \Psi(\theta)$ explicitly for large data sets.

2.2 Hessian Matrices in Deep Learning

We now consider the structure of the Hessian matrices in deep learning problems. Denote the input of the network by x_i and the output of the network by $f(x_i, \theta)$, where θ is the collection of parameters. Let $\ell(f(x_i, \theta), y_i)$ be the loss function to measure the error between the prediction $f(x_i, \theta)$ and the true label y_i . Then, the component function in (1) is: $\psi_i(\theta) := \ell_i(\theta) := \ell(f(x_i, \theta), y_i)$. By using the chain rule twice, the Hessian matrix of the objective function can be split as:

$$H(\theta) = \frac{1}{N} \sum_{i=1}^N J_f^i \nabla_f^2 \ell_i(\theta) (J_f^i)^\top, \quad (4)$$

$$\Pi(\theta) = \frac{1}{N} \sum_{i=1}^N \sum_{j=1}^m \nabla_{f_j} \ell_i(\theta) \nabla_{\theta}^2 f_j^i(\theta), \quad (5)$$

where $J_f^i = \nabla_{\theta} f(x_i, \theta) \in \mathbb{R}^{n \times m}$ and $f_j^i(\theta)$ is the j -th component of $f_i(\theta)$. The term $H(\theta)$ is also called the generalized Gauss-Newton (GGN) matrix, which is positive semi-definite (PSD) if the loss function is convex. However, the Hessian matrix (2) may not be PSD due to the term $\Pi(\theta)$.

Another type of methods is based on the Fisher information matrix (FIM). Assume that the loss function is the negative logarithm probability associated with a distribution with a density function $p(y|x, \theta)$ defined by the neural network and parameterized by θ . In general, the FIM does not coincide with the GGN matrix. However, for the square loss and the cross entropy loss function, these two matrices are equivalent. The KFAC method approximates the FIM by a block-diagonal matrix \mathbf{F} . Take an L -layer feed-forward neural network for example. Namely, each layer $j \in \{1, 2, \dots, L\}$ is given by

$$s_j = W_j a_{j-1}, \quad a_j = \phi_j(s_j),$$

where $a_0 = x$ is the input of the neural network, $a_L(x) \in \mathbb{R}^m$ is the output of the neural network under the input x , the constant term 1 is not considered in a_{j-1} for simplicity, W_j is the weight matrix and ϕ_j is the block-wise activation function. The j th diagonal block of \mathbf{F} corresponding to the parameters in the j th layer using a sample set B can be written in the following way:

$$\mathbf{F}^j := Q_{j-1, j-1} \otimes G_{j, j}, \quad (6)$$

where

$$Q_{j-1, j-1} = \frac{1}{|B|} \sum_{i \in B} a_{j-1}^i (a_{j-1}^i)^\top, \quad G_{j, j} = \frac{1}{|B|} \sum_{i \in B} \mathbb{E}_{z \sim p(z|x_i, \theta)} [g_j^i(z) g_j^i(z)^\top],$$

and $g_j^i(z) := \frac{\partial \ell(f(x_i, \theta), z)}{\partial s_j^i}$. Therefore, we can set

$$H(\theta) = \mathbf{F}. \quad (7)$$

2.3 Nyström Approximation of the Hessian

While the previous two subsections focus on the cases when the number of the data points is extremely large, we next explore the case where the dimension n is huge. In order to reduce the computational cost, an alternative way is to exploit a low-rank approximation of the Hessian. For a given symmetric matrix W , the Nyström method combining random sketching techniques can generate a symmetric low-rank matrix H . We first choose a random matrix $\Omega \in \mathbb{R}^{n \times r}$ ($r < n$), compute the matrix-matrix multiplication $Z = W\Omega$, then construct a low-rank approximation of H via

$$H \approx \mathbf{N}(W) := Z(\Omega^\top Z)^{-1}Z^\top. \quad (8)$$

Hence, the rank of $\mathbf{N}(W)$ is not larger than r . The inverse operation in (8) is replaced by the pseudoinverse if necessary. The choice of the sketching matrix Ω highly affects the quality of the approximation matrix. Each entry of Ω can be sampled i.i.d from the standard Gaussian distribution. The following theorem shown in [36] gives a bound of the Nyström approximation.

Theorem 1. *Suppose that W is a positive semi-definite matrix, W_s is the best rank- s approximation of W with $1 \leq s < r \leq n$ and Ω is a Gaussian sketching matrix. Then, we have*

$$\begin{aligned} \mathbb{E}\|\mathbf{N}(W) - W\|_1 &\leq \left(1 + \frac{s}{r-s-1}\right)\|W - W_s\|_1, \\ \mathbb{E}\|\mathbf{N}(W) - W\|_\infty &\leq \|W - W_s\|_\infty \\ &\quad + \frac{s}{r-s-1}\|W - W_s\|_1. \end{aligned}$$

For a relatively large collection of samples \mathcal{S}_H , the subsampled Newton direction using $\nabla_{\mathcal{S}_H}^2 \Psi(\theta)$ can be expensive. By using the Nyström approximation, a low-rank matrix can be generated as

$$H(\theta) = \mathbf{N}(\nabla_{\mathcal{S}_H}^2 \Psi(\theta)). \quad (9)$$

Although the original Hessian may not be low-rank, it might be helpful to capture its dominant part.

3 Structured Stochastic Quasi-Newton Methods

In this section, we describe a second-order framework for finite-sum problem (1). Take an index set $\mathcal{S}_g \subseteq \{1, 2, \dots, N\}$. The subsampled objective function values $\Psi_{\mathcal{S}_g}(\theta)$ and the subsampled gradient are:

$$\Psi_{\mathcal{S}_g}(\theta) = \frac{1}{|\mathcal{S}_g|} \sum_{i \in \mathcal{S}_g} \psi_i(\theta), \quad \nabla_{\mathcal{S}_g} \Psi(\theta) := \frac{1}{|\mathcal{S}_g|} \sum_{i \in \mathcal{S}_g} \nabla \psi_i(\theta).$$

At each iteration, a regularized quadratic approximation model at the current point θ^k is constructed as follows:

$$\min_d M_k(d) = \Psi(\theta^k) + g_k^\top d + \frac{1}{2}d^\top (B_k + \lambda_k I)d, \quad (10)$$

where $g_k = \nabla_{\mathcal{S}_g} \Psi(\theta^k)$, B_k is an estimations of the Hessian matrix of the objective function Ψ at θ^k and λ_k is the regularization parameter. By minimizing the quadratic model (10), we can obtain a direction

$$d^k = -(B_k + \lambda_k I)^{-1}g_k. \quad (11)$$

By choosing a proper step size α_k , we obtain the next iteration: $\theta^{k+1} = \theta^k + \alpha_k d^k$.

3.1 Structured quasi-Newton Matrix

The key concept is to use a quasi-Newton method to compensate the difference $\Pi(\theta^k)$ between the subsampled Hessian matrix or partial Hessian information and the real Hessian matrix. That is, the matrix B_k is constructed as

$$B_k = H_k + A_k. \quad (12)$$

Specifically, $H_k = H(\theta^k)$ can be either the subsampled Hessian matrix (3), or the GGN/FIM matrix (4), or the block diagonal KFAC matrix (7), or the Nyström approximation (9). The matrix A_k is a quasi-Newton refinement to the part $\Pi(\theta^k)$ in (2). Let $u_{k-1} = \theta^k - \theta^{k-1}$ and $\hat{v}_{k-1} = \nabla_{S_g^{k-1}} \Psi(\theta^k) - \nabla_{S_g^{k-1}} \Psi(\theta^{k-1})$. Then B_k is required to satisfy a stochastic version of the secant equation:

$$B_k u_{k-1} = (A_k + H_k) u_{k-1} = \hat{v}_{k-1},$$

which is equivalent to

$$A_k u_{k-1} = \hat{v}_{k-1} - H_k u_{k-1} := v_{k-1}.$$

3.2 Representation of the Inverse Matrix

For an efficient computation of the quasi-Newton direction d^k , we update the matrix A_k by the limited-memory quasi-Newton method [25, 34]. One widely used approach is the L-BFGS scheme. Assume that there are p pairs of vectors:

$$U_k = [u_{k-p}, \dots, u_{k-1}] \in \mathbb{R}^{n \times p}, V_k = [v_{k-p}, \dots, v_{k-1}] \in \mathbb{R}^{n \times p}. \quad (13)$$

For a given initial matrix A_k^0 , a compact representation of the L-BFGS matrix is:

$$A_k := \text{LBFGS}(U_k, V_k) = A_k^0 - C_k P_k^{-1} C_k^\top, \quad (14)$$

where

$$\begin{aligned} C_k &:= C_k(U_k, V_k) = [A_k^0 U_k, V_k] \in \mathbb{R}^{n \times 2p}, \\ P_k &:= P_k(U_k, V_k) = \begin{bmatrix} U_k^\top A_k^0 U_k & L_k \\ L_k^\top & -D_k \end{bmatrix} \in \mathbb{R}^{2p \times 2p}, \\ (L_k)_{i,j} &:= (L_k(U_k, V_k))_{i,j} \\ &= \begin{cases} u_{k-p+i-1}^\top v_{k-p+j-1} & \text{if } i > j, \\ 0 & \text{otherwise,} \end{cases} \\ D_k &= D_k(U_k, V_k) = \text{diag} [u_{k-p}^\top v_{k-p}, \dots, u_{k-1}^\top v_{k-1}]. \end{aligned}$$

The initial matrix A_k^0 is usually set to be a positive scalar γ_k times the identity matrix, i.e., $\gamma_k I$. One may even apply the Nyström technique again to provide a low-rank approximation. Note that the two-loop recursion of the L-BFGS (Algorithm 7.4 in [25]) is based on the approximation to the inverse of the Hessian. It takes H_k in an equation for an initial direction. However, the scheme (14) targets at the Hessian directly.

In order to ensure the positive definiteness of A_k , the pair $\{u_i, v_i\}$ should satisfy $u_i^\top v_i \geq \epsilon_B \|u_i\|_2 \|v_i\|_2$ with a small constant, say $\epsilon_B = 10^{-8}$. Although H_k may not be positive definite due to the non-convexity of the functions $\psi_i(\theta)$, the regularization parameter λ_k can be adjusted suitably such that both H_k and B_k have good properties to generate descent directions.

We now compute the inverse of $(B_k + \lambda_k I)$. Let $\tilde{H}_k = H_k + A_k^0 + \lambda_k I$. Assume that \tilde{H}_k is invertible. Otherwise, the regularization parameter λ_k can be tuned accordingly. By using the Sherman-Morrison-Woodbury formula, we obtain

$$(B_k + \lambda_k I)^{-1} = (\tilde{H}_k - C_k P_k^{-1} C_k^\top)^{-1} = \tilde{H}_k^{-1} + \tilde{H}_k^{-1} C_k T_k^{-1} C_k^\top \tilde{H}_k^{-1}, \quad (15)$$

where $T_k = P_k - C_k^\top \tilde{H}_k^{-1} C_k$. Note that the main computational cost in (15) is the inverse of \tilde{H}_k . Fortunately, the special structures of the matrices H_k and A_k^0 still allow an efficient evaluation in several cases, for example, if H_k is the KFAC matrix (7) and A_k^0 is a simple diagonal matrix.

Our strategy can also be easily extended to the case when $B_k = \text{diag}\{B_k^1, \dots, B_k^L\}$ is a block diagonal matrix. One can require that the j -th block of A_k satisfies the following secant equation: $A_k^j u_{k-1}^j = \hat{v}_{k-1}^j - H_k^j u_{k-1}^j := v_{k-1}^j$, where u_{k-1}^j and v_{k-1}^j are the sub-vector of u_{k-1} and v_{k-1} corresponding to the j -th block.

3.3 Explicit Inverse by Low-Rank Structures

We now assume that $H_k = Q_k Q_k^\top$ is a low-rank matrix, where $Q_k \in \mathbb{R}^{n \times r}$, $r \ll n$. An example is the Nyström approximation (9) by setting $Q_k = Z(\Omega^\top Z)^{-1/2}$. For convenience of notation, we write:

$$\tilde{A}_k = A_k^0 + \lambda_k I, \quad \tilde{P}_k = \begin{bmatrix} P_k^{-1} & 0 \\ 0 & -I \end{bmatrix}, \quad \tilde{C}_k = [C_k, Q_k].$$

Then the Sherman-Morrison-Woodbury formula again yields:

$$(B_k + \lambda_k I)^{-1} = (\tilde{A}_k^0 - \tilde{C}_k \tilde{P}_k^{-1} \tilde{C}_k^\top)^{-1} = \tilde{A}_k^{-1} + \tilde{A}_k^{-1} \tilde{C}_k \hat{T}_k^{-1} \tilde{C}_k^\top \tilde{A}_k^{-1},$$

where $\hat{T}_k = \tilde{P}_k - \tilde{C}_k^\top \tilde{A}_k^{-1} \tilde{C}_k$. Therefore, the computational cost of the inverse matrix can be much smaller than the original operation as long as the rank is kept low.

3.4 Extra-Step Strategy

In the quasi-Newton update process, we may compute the stochastic gradient twice at the same sampling sets \mathcal{S}_g^k with respect to two points. To make full use of these gradients, it might be helpful to add an extra-gradient step similar to [40]. Specifically, the update process is changed as follows:

$$z^k = \theta^k - \alpha_k (B_k + \lambda_k I)^{-1} \nabla_{\mathcal{S}_g^k} \Psi(\theta^k), \quad \theta^{k+1} = z^k - \beta_k \nabla_{\mathcal{S}_g^k} \Psi(z^k), \quad (16)$$

where α_k, β_k are the step sizes and the pairs (13) are modified with

$$u_k = z^k - \theta^k, \quad \hat{v}_k = \nabla_{\mathcal{S}_g^k} \Psi(z^k) - \nabla_{\mathcal{S}_g^k} \Psi(\theta^k). \quad (17)$$

This strategy reuses the subsampled gradient in the quasi-Newton scheme and the computational cost is saved. Although $\nabla_{\mathcal{S}_g^k} \Psi(z^k)$ is a biased estimation to the gradient, one can assume that the noise is bounded so that the convergence can still be guaranteed.

3.5 Damping Strategy

In order to decide whether the regularization parameter should be updated or not, we calculate a ratio between the actual reduction of the subsampled objective function $\Psi_{\mathcal{S}_g^k}(\theta)$ and the predicted reduction of $M_k(d)$:

$$\rho_k = \frac{\Psi_{\mathcal{S}_g^k}(\theta^k + d^k) - \Psi_{\mathcal{S}_g^k}(\theta^k)}{M_k(d^k)}. \quad (18)$$

Then the regularization parameter λ_{k+1} is updated as

$$\lambda_{k+1} \in \begin{cases} (0, \lambda_k] & \text{if } \rho_k > \eta_2, \\ [\lambda_k, \zeta_1 \lambda_k] & \text{if } \eta_1 \leq \rho_k \leq \eta_2, \\ [\zeta_1 \lambda_k, \zeta_2 \lambda_k] & \text{otherwise,} \end{cases} \quad (19)$$

where $0 < \eta_1 \leq \eta_2 < 1$ and $1 < \zeta_1 \leq \zeta_2$. Similar strategies are common in deterministic second-order methods.

3.6 Extensions

Our proposed method is general and several other techniques can be integrated into the framework. We next mention a few possible extensions.

Different stochastic quasi-Newton schemes. In addition to the BFGS type method, stochastic methods based on the limited-memory symmetric rank-one (SR1) update are also possible. Let $\tilde{V}_k = V_k - A_k^0 U_k$. Then, we can compute

$$A_{k+1} = A_k^0 + \tilde{V}_k (D_k + L_k + L_k^\top - U_k^\top A_k^0 U_k)^{-1} \tilde{V}_k^\top, \quad (20)$$

Algorithm 1: Stochastic Quasi-Newton Method

- 1 Initialization: Choose an initial point θ^0 . Select step sizes (α_k) , (β_k) . Set the memory size p .
for $k = 0, 1, \dots$ **do**
 - 2 Choose the random sample sets $\mathcal{S}_g^k, \mathcal{S}_H^k \subset [N]$. Compute $\nabla_{\mathcal{S}_g^k} \Psi(\theta^k)$ and H_k . Set the parameter λ_k .
 - 3 Compute the matrix $A_k = \text{LBFGS}(U_k, V_k)$.
 - 4 Compute the direction d^k and perform $z^k = \theta^k + \alpha_k d^k$.
 - 5 Compute the gradient $\nabla_{\mathcal{S}_g^k} \Psi(z^k)$ with the same samples and update the pairs (U_k, V_k) .
 - 6 **OPTION I:** Perform and update the extra step $\theta^{k+1} = z^k - \beta_k \nabla_{\mathcal{S}_g^k} \Psi(z^k)$.
 OPTION II: Set $\theta^{k+1} := z^k$.
-

where the matrices U_k, V_k, D_k and L_k are the same as these in (14). A multi-batch update for the pairs (U_k, V_k) is used in [3]. The powell-damping strategy is studied in [38], and etc.

Variance Reduction Techniques. The variance reduction methods can often provide a better estimation to the gradient and improve the performance of the algorithm. They can also be applied to our stochastic quasi-Newton methods in a natural way.

4 Theoretical Analysis

4.1 Global Convergence

In this part, we consider the extra-step iteration in (16) and give a general analysis for our stochastic extra-step quasi-Newton method. When $\beta_k = 0$, the method becomes the pure stochastic quasi-Newton method. When there is no A_k , the method degenerates to the subsampled Newton method. It is obvious that our analysis fits both cases. Our analysis simplifies these arguments in [40] since we consider the smooth case.

According to the stochastics in the iteration (16), we can define a filtration \mathcal{F}_k such that $\theta^k \in \mathcal{F}_{k-1}$ and H_k and $\nabla_{\mathcal{S}_g^k} \Psi(\theta^k)$ are \mathcal{F}_{k-1} -independent. A few necessary assumptions are listed below.

Assumption 2. A.1) Ψ is continuously differentiable on \mathbb{R}^n and is bounded from below. The gradient $\nabla \Psi$ is Lipschitz continuous on \mathbb{R}^n with modulus $L_\Psi \geq 1$.

A.2) For any iteration k , we assume that B_k and $\nabla_{\mathcal{S}_g^k} \Psi(\theta^k)$ are \mathcal{F}_{k-1} -independent and it holds almost surely that

$$\mathbb{E}[\nabla_{\mathcal{S}_g^k} \Psi(\theta^k) | \mathcal{F}_{k-1}] = \nabla \Psi(\theta^k), \quad \mathbb{E}[\|\nabla_{\mathcal{S}_g^k} \Psi(\theta^k) - \nabla \Psi(\theta^k)\|^2 | \mathcal{F}_{k-1}] \leq \sigma_k^2.$$

A.3) For any iteration k , we assume almost surely

$$\mathbb{E}[\|\nabla_{\mathcal{S}_g^k} \Psi(z_k) - \nabla \Psi(z_k)\|^2 | \mathcal{F}_{k-1}] \leq \sigma_{k,+}^2.$$

A.4) There exists two positive constants h_1, h_2 such that

$$h_1 I \preceq (B_k + \lambda_k I)^{-1} \preceq h_2 I$$

for all k .

The above assumptions are common and standard in stochastic quasi-Newton type methods [11, 5, 3, 38, 40]. In the structured curvature matrix, the cheap part H_k is \mathcal{F}_{k-1} -independent of $\nabla_{\mathcal{S}_g^k} \Psi(\theta^k)$ and $A_k \in \mathcal{F}_{k-1}$. It is also obvious that $B_k + \lambda_k I$ and $\nabla_{\mathcal{S}_g^k} \Psi(\theta^k)$ are \mathcal{F}_{k-1} -independent.

Theorem 3. Suppose that Assumptions A.1-A.3 are satisfied and the step sizes $(\alpha_k)_k$ and $(\beta_k)_k$ are chosen as follows:

$$\alpha_k \leq \min \left\{ \frac{1}{L_\Psi}, \frac{h_1}{4h_2^2 L_\Psi} \right\}, \quad \beta_k \leq \min \left\{ \frac{\alpha_k}{4}, \frac{h_1 \alpha_k}{8} \right\}. \quad (21)$$

Then, under the conditions:

$$\sum \alpha_k = \infty, \sum \alpha_k \sigma_k^2 < \infty, \sum \alpha_k \sigma_{k,+}^2 < \infty, \quad (22)$$

it holds for Algorithm 1 almost surely that

$$\lim_{k \rightarrow \infty} \mathbb{E} \|\nabla \Psi(\theta^k)\| = 0 \text{ and } \lim_{k \rightarrow \infty} \nabla \Psi(\theta^k) = 0.$$

The proof is shown in Appendix C.

We next show the iteration complexity of our method.

Theorem 4. *Suppose that the same assumptions hold as Theorem 3 and the step size α_k is set to $\alpha_k = \varsigma \cdot k^{-v}$, where $\varsigma = \min \left\{ \frac{1}{L_\Psi}, \frac{h_1}{4h_2^2 L_\Psi} \right\}$ and $v \in (0.5, 1)$. If the variances $\sigma_k^2, \sigma_{k,+}^2$ satisfy $\max\{\sigma_k^2, \sigma_{k,+}^2\} \leq c \cdot k^{-\chi}$ with a constant c and $1 - v < \chi < 1$, then the number of iterations l to guarantee*

$$\frac{1}{l} \sum_{k=1}^l \mathbb{E} \|\nabla \Psi(\theta^k)\|^2 \leq \epsilon \in (0, 1)$$

is at most $\mathcal{O}(\epsilon^{-\frac{1}{1-v}})$.

The proof is shown in Appendix D.

4.2 Local Convergence

In this part, we analyze the convergence property of the stochastic quasi-Newton method under the stochastic Dennis-Moré condition in a small local region of an optimal solution. In fact, the parameter λ_k should converge to zero in this region. Hence, we consider a simplified scheme:

$$\theta^{k+1} = \theta^k - B_k^{-1} \nabla_{\mathcal{S}_g^k} \Psi_k(\theta^k). \quad (23)$$

We make the following assumptions.

Assumption 5. *B.1) The Hessian $\nabla^2 \Psi(\theta)$ is continuous at a local optimal point θ^* and $\nabla^2 \Psi(\theta^*)$ is nonsingular.*

B.2) The point θ^k converges to θ^ almost surely.*

B.3) The term $\lim_{k \rightarrow \infty} \frac{\|(A_k + H_k - \nabla^2 \Psi(\theta^))(\theta^{k+1} - \theta^k)\|}{\|\theta^{k+1} - \theta^k\|} = 0$ holds almost surely.*

Then our local convergence is summarized as follows.

Theorem 6. *Suppose that Assumptions A.2 and B.1-B.3 hold. Let η_k, p_k be sequences with $\eta_k \rightarrow 0$, $\eta_k \geq \eta_{k+1}$ and $\sum_{k=1}^{\infty} p_k < \infty$. If σ_k satisfies $\sigma_k^2 \leq c \eta_k^k p_k$, where c is a constant, then the sequence $\{\theta^k\}$ generated by (23) converges r -superlinearly to θ^* almost surely.*

The proof is shown in Appendix E.

Assumption B.3 is the critical assumption in our analysis. It is an extension of the Dennis-Moré condition in the stochastic case. It may be satisfied if the optimization problem has a good property and the sample size is large enough. We next show that Assumption B.3 holds for the method using the Nyström approximation in Section 2.3, i.e., setting

$$H_k = \mathbf{N} \left(\nabla_{\mathcal{S}_H^k}^2 \Psi(\theta^k) \right). \quad (24)$$

Let $\Omega_k \in \mathbb{R}^{n \times r_k}$ be the Gaussian sketching matrix in the k -th iteration and $[\nabla_{\mathcal{S}_H^k}^2 \Psi(\theta^k)]_{s_k}$ be the best rank- s_k approximation of $\nabla_{\mathcal{S}_H^k}^2 \Psi(\theta^k)$ with $2 \leq s_k + 1 < r_k \leq n$.

A few additional assumptions are needed.

Assumption 7. C.1) For any iteration k , we assume

$$\mathbb{E}[\nabla_{S_H^k}^2 \Psi(\theta^k) | \mathcal{F}_{k-1}] = \nabla^2 \Psi(\theta^k), \quad \mathbb{E}[\|\nabla_{S_H^k}^2 \Psi(\theta^k) - \nabla^2 \Psi(\theta^k)\|^2 | \mathcal{F}_{k-1}] \leq \omega_k^2.$$

C.2) The matrix $\nabla_{S_H^k}^2 \Psi(\theta^k)$ is positive semi-definite.

C.3) The term $\lim_{k \rightarrow \infty} \frac{\|A_k(\theta^{k+1} - \theta^k)\|}{\|\theta^{k+1} - \theta^k\|} = 0$ holds almost surely.

Proposition 8. Suppose that Assumptions C.1-C.3 hold. Let γ_k be sequence with $\gamma_k \rightarrow 0$, and p_k be a sequence with $\sum_{k=1}^{\infty} p_k < \infty$. If $\|\nabla_{S_H^k}^2 \Psi(\theta^k) - [\nabla_{S_H^k}^2 \Psi(\theta^k)]_{s_k}\|_1 \leq \gamma_k p_k$ and $\omega_k^2 \leq \gamma_k p_k$, then Assumption B.3 holds for the sequence $\{\theta^k\}$ generated by (23) with the Nyström approximation (24).

The proof is shown in Appendix F.

The condition $\omega_k^2 \leq \gamma_k p_k$ can be satisfied if the sample size is large enough, while $\|\nabla_{S_H^k}^2 \Psi(\theta^k) - [\nabla_{S_H^k}^2 \Psi(\theta^k)]_{s_k}\|_1 \leq \gamma_k p_k$ means that the matrix $\nabla_{S_H^k}^2 \Psi(\theta^k)$ is dominated by the part associated with a few largest eigenvalues. Similar arguments can be used to analyze the case where H_k is the subsampled Hessian matrix or the FIM matrix.

5 Numerical Experiments

In this section, we compare our proposed method with a few standard methods for binary classification, deep autoencoders and neural networks. All methods used in the experiments are briefly listed below and their detailed implementation is reported in Appendix A. **SGD** is the stochastic gradient method. **L-BFGS** is the well-known limited-memory quasi-Newton method. **SL-SR1** is the sampled L-SR1 method. **SSN** is the subsampled Newton method. **KFAC** is a method using the Fisher matrix for deep learning problems. **S4QN**, **SKQN** and **SKQNE** are the variants of our stochastic quasi-Newton method using the subsampled Hessian and the KFAC matrix without and with the extra-gradient steps, respectively.

5.1 Binary Classification

In this part, we consider logistic regression problems for binary classification:

$$\min_{x \in \mathbb{R}^n} \Psi(x) = \frac{1}{N} \sum_{i=1}^N \log(1 + \exp(-b_i \langle a_i, x \rangle)) + \mu \|x\|_2^2, \quad (25)$$

where $\{a_i, b_i\} \in \mathbb{R}^n \times \{-1, 1\}$, $i \in [N]$ correspond to a given dataset. The statistics of the datasets used in our numerical comparisons are listed in Appendix B.1.

We compare S4QN with SGD, SSN and L-BFGS. Let one epoch be a full pass through the dataset and define the relative error between the final objective function value and the optimal function value Ψ^* as $\text{rel_err} := (\Psi(\theta) - \Psi^*) / \max\{1, \Psi^*\}$. The change of the relative error with respect to the number of epochs for `rcv1` and `news20` is shown in Figure 1 and other experiments are reported in Appendix B.1 for space.

We can observe that S4QN outperforms the other methods greatly. It is worth emphasizing that all settings of S4QN are the same as SSN except an additional quasi-Newton matrix. The sample size of the gradient estimation is increasing and it becomes the full gradient in the last stage. S4QN exhibits a faster local convergence rate than other methods. These facts illustrate that the structured methods can accelerate the Hessian-based and quasi-Newton methods.

5.2 Deep Autoencoders

We next consider the deep autoencoder problem with the same architectures on three datasets: “MNIST”, “CURVES” and “FACES” [16]. The layer sizes are D -1000-500-250-30-250-500-1000- D ,

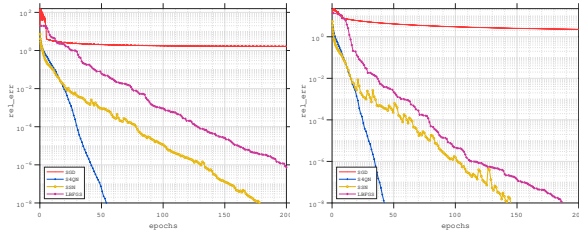


Figure 1: Binary classification: rcv1 (left) and new20 (right).

where D is the dimension of the input data. We use the cross-entropy loss for CURVES and MNIST, and the square error loss for FACES. We compare SKQNE and SKQN with SGD and KFAC whose implementation details are reported in Appendix A. We report the change of the training loss and testing loss versus epochs on MNIST in Figure 2 and the other results in Appendix B.2.

Compared to the first-order method SGD, the second-order methods are better and stabler on all three datasets. In comparison to KFAC, our proposed methods have an improvement in both the training loss and testing loss while the computational cost does not increase much at each iteration. Our results suggest that the structured quasi-Newton method with more Hessian information accelerates the convergence.

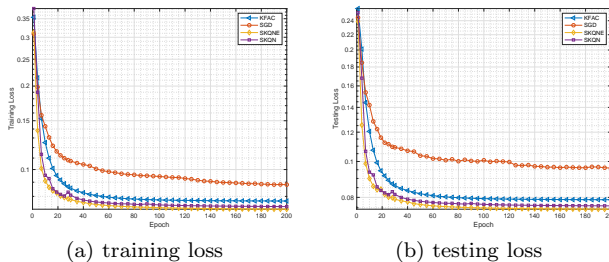


Figure 2: Autoencoders: training and testing loss of MNIST.

5.3 Toy Neural Network

In this subsection, we consider a toy classification problem [2] using deep neural networks. The synthetic dataset consists of 50 points from each of two curves: $\sin(8\theta)$, $\sin(8\theta) + 0.8$, where $\theta \in [0, 1]$. This classification is more difficult than the original setting in [2]. The fully connected neural networks are trained in small, medium and large scales with four hidden layers and the sigmoid function as the activation. The statistics of architectures are summarized in Appendix B.3.

The change of the training loss and training accuracy are reported in Figure 3 and Appendix B.3. It is obvious that the performance of SKQN is much better than other methods. In particular, the training loss can be much smaller and is reduced to the order of 10^{-1} around 50 epochs. The training accuracy reaches 95% and 100% in less than fifty and eighty epochs, respectively.

5.4 Deep CNN

We next consider the “ResNet-18” [14] with the cross-entropy loss on two datasets “CIFAR-10” and “ImageNette”. CIFAR-10 consists of 50,000 training and 10,000 testing images. ImageNette is a subset of Imagenet-1000, consisting 12,800 images from 10 classes.

The changes of the training loss and testing accuracy versus epoch of CIFAR-10 are reported in Figure 4. We can see that the second-order type methods outperform the first-order type

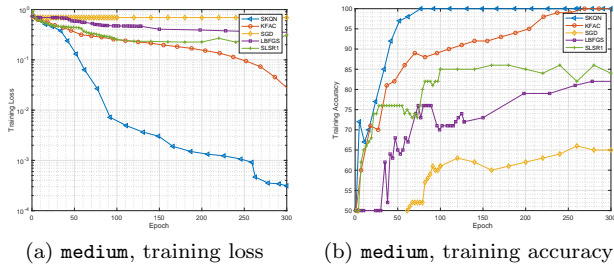


Figure 3: Toy neural network: medium.

methods in terms of the testing accuracy. The training error of our proposed quasi-Newton methods decreases faster than that of KFAC while the testing accuracy of them is at least comparable.

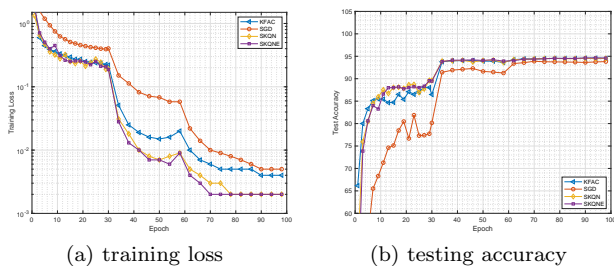


Figure 4: Deep CNN: CIFAR-10.

6 Conclusion

In this paper, a novel stochastic structured quasi-Newton framework is proposed and analyzed for large-scale nonconvex finite-sum optimization problems. Our methods refine the quasi-Newton method using the partial Hessian information. The quasi-Newton direction can be computed explicitly by using a low-rank update from the Nyström approximation. We obtain global convergence to stationary points in expectation if the step sizes and the stochastic variances satisfy some certain conditions. A local r -superlinear convergence rate is analyzed under some mild conditions. Our experimental results demonstrate the efficiency of our structured stochastic quasi-Newton methods. In the future, we will implement our method on MindSpore¹, a unified training and inference framework for device, edge and cloud in Huawei’s full-stack, all-scenario AI portfolio.

References

- [1] Zeyuan Allen-Zhu. Katyusha: The first direct acceleration of stochastic gradient methods. *Journal of Machine Learning Research*, 18(221):1–51, 2018.
- [2] Albert S Berahas, Majid Jahani, and Martin Takáč. Quasi-newton methods for deep learning: Forget the past, just sample. *ArXiv:1901.09997*, 2019.
- [3] Albert S Berahas, Jorge Nocedal, and Martin Takáč. A multi-batch l-bfgs method for machine learning. In *Advances in Neural Information Processing Systems*, pages 1055–1063, 2016.

¹<https://gitee.com/mindspore/>

- [4] Aleksandar Botev, Hippolyt Ritter, and David Barber. Practical Gauss-Newton optimisation for deep learning. In *International Conference on Machine Learning*, pages 557–565, 2017.
- [5] R. H. Byrd, S. L. Hansen, Jorge Nocedal, and Y. Singer. A stochastic quasi-Newton method for large-scale optimization. *SIAM Journal on Optimization*, 26(2):1008–1031, 2016.
- [6] Richard H Byrd, Gillian M Chin, Will Neveitt, and Jorge Nocedal. On the use of stochastic Hessian information in optimization methods for machine learning. *SIAM Journal on Optimization*, 21(3):977–995, 2011.
- [7] Patrick L Combettes and Jean-Christophe Pesquet. Proximal splitting methods in signal processing. In *Fixed-point algorithms for inverse problems in science and engineering*, pages 185–212. Springer, 2011.
- [8] Li Deng and Dong Yu. Deep learning: Methods and applications. *Found. and Trends® Signal Process.*, 7(3–4):197–387, June 2014.
- [9] John Duchi, Elad Hazan, and Yoram Singer. Adaptive subgradient methods for online learning and stochastic optimization. *Journal of Machine Learning Research*, 12:2121–2159, 2011.
- [10] Ian Goodfellow, Yoshua Bengio, and Aaron Courville. *Deep Learning*. MIT Press, 2016.
- [11] Robert Gower, Donald Goldfarb, and Peter Richtárik. Stochastic block bfgs: Squeezing more curvature out of data. In *International Conference on Machine Learning*, pages 1869–1878, 2016.
- [12] Priya Goyal, Piotr Dollár, Ross Girshick, Pieter Noordhuis, Lukasz Wesolowski, Aapo Kyrola, Andrew Tulloch, Yangqing Jia, and Kaiming He. Accurate, large minibatch SGD: Training ImageNet in 1 hour. ArXiv:1706.02677, 2017.
- [13] Trevor Hastie, Robert Tibshirani, and Jerome Friedman. *The elements of statistical learning: data mining, inference, and prediction*. Springer-Verlag, New York, 2001.
- [14] Kaiming He, Xiangyu Zhang, Shaoqing Ren, and Jian Sun. Deep residual learning for image recognition. In *IEEE Conference on Computer Vision and Pattern Recognition*, pages 770–778, 2016.
- [15] João F Henriques, Sebastien Ehrhardt, Samuel Albanie, and Andrea Vedaldi. Small steps and giant leaps: Minimal newton solvers for deep learning. In *IEEE International Conference on Computer Vision*, pages 4763–4772, 2019.
- [16] Geoffrey E Hinton and Ruslan R Salakhutdinov. Reducing the dimensionality of data with neural networks. *Science*, 313(5786):504–507, 2006.
- [17] Jiang Hu, Bo Jiang, Lin Lin, Zaiwen Wen, and Ya-xiang Yuan. Structured quasi-newton methods for optimization with orthogonality constraints. *SIAM Journal on Scientific Computing*, 41(4):A2239–A2269, 2019.
- [18] Rie Johnson and Tong Zhang. Accelerating stochastic gradient descent using predictive variance reduction. In *Advances in Neural Information Processing Systems*, pages 315–323, 2013.
- [19] Diederik P Kingma and Jimmy Ba. Adam: A method for stochastic optimization. *ArXiv:1412.6980*, 2014.
- [20] Yann LeCun, Yoshua Bengio, and Geoffrey Hinton. Deep learning. *Nature*, 521:436–444, 2015.
- [21] James Martens. Deep learning via Hessian-free optimization. In *International Conference on Machine Learning*, pages 735–742, 2010.
- [22] James Martens and Roger Grosse. Optimizing neural networks with kronecker-factored approximate curvature. In *International Conference on Machine Learning*, pages 2408–2417, 2015.

- [23] Andre Milzarek, Xiantao Xiao, Shicong Cen, Zaiwen Wen, and Michael Ulbrich. A stochastic semismooth newton method for nonsmooth nonconvex optimization. *SIAM Journal on Optimization*, 29(4):2916–2948, 2019.
- [24] Lam M Nguyen, Jie Liu, Katya Scheinberg, and Martin Takáč. SARAH: A novel method for machine learning problems using stochastic recursive gradient. In *International Conference on Machine Learning*, pages 2613–2621, 2017.
- [25] Jorge Nocedal and Stephen J Wright. *Numerical Optimization*. Springer, New York, 2006.
- [26] Kazuki Osawa, Yohei Tsuji, Yuichiro Ueno, Akira Naruse, Rio Yokota, and Satoshi Matsuoka. Large-scale distributed second-order optimization using kronecker-factored approximate curvature for deep convolutional neural networks. In *IEEE Conference on Computer Vision and Pattern Recognition*, pages 12359–12367, 2019.
- [27] Mert Pilanci and Martin J Wainwright. Newton sketch: A near linear-time optimization algorithm with linear-quadratic convergence. *SIAM Journal on Optimization*, 27(1):205–245, 2017.
- [28] Herbert Robbins and Sutton Monro. A stochastic approximation method. *The Annals of Mathematical Statistics*, 22:400–407, 1951.
- [29] Fred Roosta and Michael W. Mahoney. Sub-sampled newton methods. *Mathematical Programming*, 174:293–326, 2019.
- [30] Jürgen Schmidhuber. Deep learning in neural networks: An overview. *Neural Networks*, 61:85–117, 2015.
- [31] Nicol N Schraudolph. Fast curvature matrix-vector products for second-order gradient descent. *Neural computation*, 14(7):1723–1738, 2002.
- [32] Nicol N Schraudolph, Jin Yu, and Simon Günter. A stochastic quasi-newton method for online convex optimization. In *International Conference on Artificial Intelligence and Statistics*, pages 436–443, 2007.
- [33] Karen Simonyan and Andrew Zisserman. Very deep convolutional networks for large-scale image recognition. In *International Conference on Learning Representations*, 2015.
- [34] Wenyu Sun and Ya-Xiang Yuan. *Optimization theory and methods: nonlinear programming*. Springer US, 2006.
- [35] Ilya Sutskever, James Martens, George Dahl, and Geoffrey Hinton. On the importance of initialization and momentum in deep learning. In *International Conference on Machine Learning*, pages 1139–1147, 2013.
- [36] Joel A. Tropp, Alp Yurtsever, Madeleine Udell, and Volkan Cevher. Fixed-rank approximation of a positive-semidefinite matrix from streaming data. In *Neural Information Processing Systems*, page 1225–1234, 2017.
- [37] Vladimir Vapnik. *The nature of statistical learning theory*. Springer-Verlag, New York, 2013.
- [38] Xiao Wang, Shiqian Ma, Donald Goldfarb, and Wei Liu. Stochastic Quasi-Newton Methods for Nonconvex Stochastic Optimization. *SIAM Journal on Optimization*, 27(2):927–956, 2017.
- [39] Peng Xu, Fred Roosta, and Michael W. Mahoney. Newton-type methods for non-convex optimization under inexact Hessian information. *Mathematical Programming*, May 2019.
- [40] Minghan Yang, Andre Milzarek, Zaiwen Wen, and Tong Zhang. A stochastic extra-step quasi-newton method for nonsmooth nonconvex optimization. *ArXiv:1910.09373*, 2019.
- [41] Yang You, Zhao Zhang, Cho-Jui Hsieh, James Demmel, and Kurt Keutzer. ImageNet training in minutes. In *International Conference on Parallel Processing*, pages 1–10, 2018.

Appendix

A. Implementation Details

- **SGD** is the stochastic gradient method with or without momentum. The step size α_0 is fixed by grid search in $\{0.01, 0.05, 0.1, 0.2, 0.4, 0.6, 0.8, 1, 2, 8\}$. The momentum parameter is set to be 0 for binary classifications and 0.9 otherwise. The batch size is set to 1 for logistic regression, 100 for the toy neural network, 512 for MNIST and CURVES and 2048 for FACES, 256 for deep CNN problems. The learning rate is determined by the Armijo line search in the toy neural network, is fixed to $\eta = \alpha_0$ in deep autoencoder and is set to $\eta = \alpha_0 \times 0.1^{\lfloor \text{epoch}/30 \rfloor}$ for deep CNN.
- **L-BFGS** is the well-known limited memory quasi-Newton method.
- **SL-SR1** is the sampled version of L-SR1 method² and the default parameters are used.
- **SSN** is the subsampled Newton method. The batch size \mathcal{S}_H for the subsampled Hessian matrix is $\min\{2000, \lfloor 0.01N \rfloor\}$. The batch size of the subsampled gradient $|\mathcal{S}_g|$ is changing as $\min\{|\mathcal{S}_g| \cdot 1.1, N\}$.
- **KFAC** is a method approximating the Fisher matrix. For the toy neural network, the learning rate is determined by the Armijo’s backtracking line search tuned independently for each network. The momentum parameter is set to 0 and the curvature matrix is recomputed every iteration. For deep autoencoder, the learning rate is set to $\eta = \beta^{\text{epoch}}$ with $\beta = 0.98$ for MNIST, and 1 for CURVES and FACES. The damping parameters and the momentum parameter are set to 0.2, 0.9 respectively. The curvature matrix is evaluated every 5 iterations. For deep CNN, the learning rate is set to $\eta = 0.1 \times 0.1^{\lfloor \text{epoch}/30 \rfloor}$. The damping parameters and the momentum parameter are set to 0.8, 0.9, respectively. The curvature matrix is evaluated every 50 iterations.
- **S4QN** denotes our structured stochastic quasi-Newton method with partial Hessian information. The set up of the subsampled Hessian H_k is the same as SSN. The matrix A_k is generated by the stochastic L-BFGS method and the memory size is 5.
- **SKQN** denotes our structured stochastic quasi-Newton method using the block diagonal KFAC matrix. The memory size is 10 for the toy neural network and 5 otherwise. **SKQNE** is the variant with the extra-gradient steps.

B. Additional Experiments

B.1. Binary Classification

See Figure 5.

B.2. Deep Autoencoders

See Figure 6.

B.3. Toy Neural Network

See Figure 7.

²The source code of SL-SR1 is downloadable from <https://github.com/OptMLGroup/SQN>

Table 1: A description of the datasets on binary classification.

data set	N	n
spam	92189	823470
realsim	72,309	20958
covtype	581012	54
rcv1	20242	47236
news20	19996	1355191
ijcnn1	49900	22

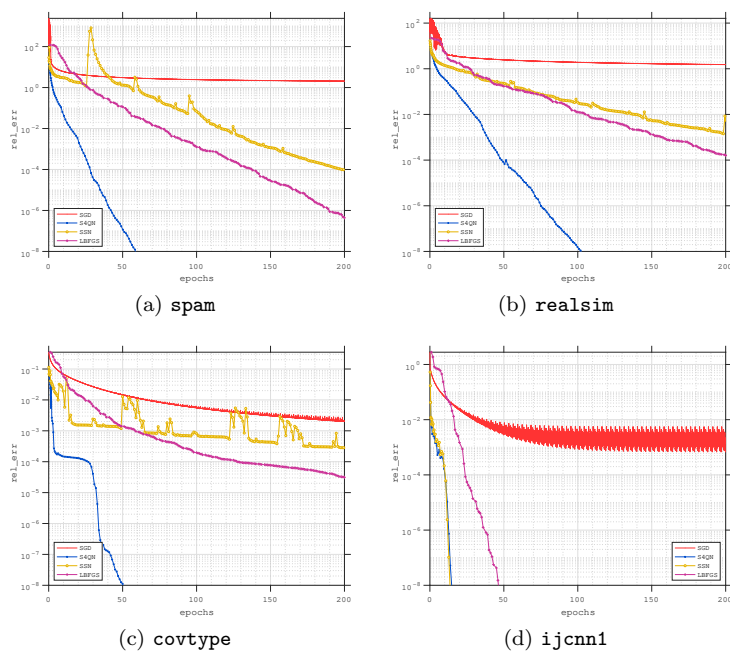


Figure 5: Binary classification: Iteration history of the relative difference to the optimal function values versus epochs.

B.4. Deep CNN

See Figure 8.

C. Proof of Theorem 3

Proof. It follows from Assumption A.1 that the descent property holds:

$$\Psi(y) \leq \Psi(x) + \langle \nabla \Psi(x), y - x \rangle + \frac{L_\Psi}{2} \|y - x\|^2. \quad (26)$$

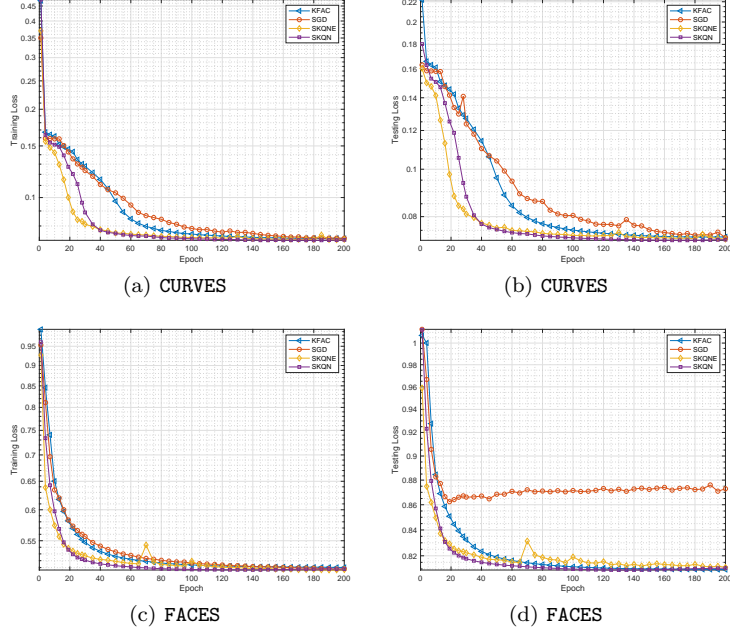


Figure 6: Autoencoder: training loss (left) and testing loss(right) versus epochs

Table 2: The detail of the toy neural network.

Network	Architecture	Dimension
small	2-2-2-2-2	36
medium	2-4-8-8-4-2	176
large	2-10-20-20-10-2	908

Applying (26) and the Young inequality, we obtain for any $\tau_k > 0$:

$$\begin{aligned}
\Psi(\theta^{k+1}) - \Psi(\theta^k) &\leq \langle \nabla \Psi(\theta^k), \theta^{k+1} - \theta^k \rangle + \left(\frac{L_\Psi}{2}\right) \|\theta^{k+1} - \theta^k\|^2 \\
&= \langle \nabla \Psi(\theta^k), -\alpha_k (B_k + \lambda_k I)^{-1} \nabla_{S_g^k} \Psi(\theta^k) - \beta_k \nabla_{S_g^k} \Psi(z^k) \rangle \\
&\quad + \frac{L_\Psi}{2} \|\alpha_k (B_k + \lambda_k I)^{-1} \nabla_{S_g^k} \Psi(\theta^k) + \beta_k \nabla_{S_g^k} \Psi(z^k)\|^2 \\
&\leq \langle \nabla \Psi(\theta^k), -\alpha_k (B_k + \lambda_k I)^{-1} \nabla_{S_g^k} \Psi(\theta^k) \rangle + \frac{\tau_k}{2} \|\nabla \Psi(\theta^k)\|^2 \\
&\quad + \left(\frac{\beta_k^2}{2\tau_k} + L_\Psi \beta_k^2\right) \|\nabla_{S_g^k} \Psi(z^k)\|^2 + L_\Psi \alpha_k^2 h_2^2 \|\nabla_{S_g^k} \Psi(\theta^k)\|^2.
\end{aligned} \tag{27}$$

Next, by using the Young inequality twice and the Lipschitz property of $\nabla \Psi$, we have:

$$\begin{aligned}
\|\nabla_{S_g^k} \Psi(z^k)\|^2 &= \|\nabla_{S_g^k} \Psi(z^k) - \nabla \Psi(z^k) + \nabla \Psi(z^k) - \nabla \Psi(\theta^k) + \nabla \Psi(\theta^k)\|^2 \\
&\leq 2\|\nabla_{S_g^k} \Psi(z^k) - \nabla \Psi(z^k)\|^2 + 4L_\Psi^2 \alpha_k^2 h_2^2 \|\nabla_{S_g^k} \Psi(\theta^k)\|^2 + 4\|\nabla \Psi(\theta^k)\|^2.
\end{aligned} \tag{28}$$

Using the similar idea, taking conditional expectation based on \mathcal{F}_{k-1} together with $\mathbb{E}[\nabla_{S_g^k} \Psi(\theta^k) | \mathcal{F}_{k-1}] = \nabla \Psi(\theta^k)$ yields

$$\begin{aligned}
\mathbb{E}[\|\nabla_{S_g^k} \Psi(\theta^k)\|^2 | \mathcal{F}_{k-1}] &= \mathbb{E}[\|\nabla_{S_g^k} \Psi(\theta^k) - \nabla \Psi(\theta^k) + \nabla \Psi(\theta^k)\|^2 | \mathcal{F}_{k-1}] \\
&\leq \mathbb{E}[\|\nabla_{S_g^k} \Psi(\theta^k) - \nabla \Psi(\theta^k)\|^2 | \mathcal{F}_{k-1}] + \|\nabla \Psi(\theta^k)\|^2.
\end{aligned} \tag{29}$$

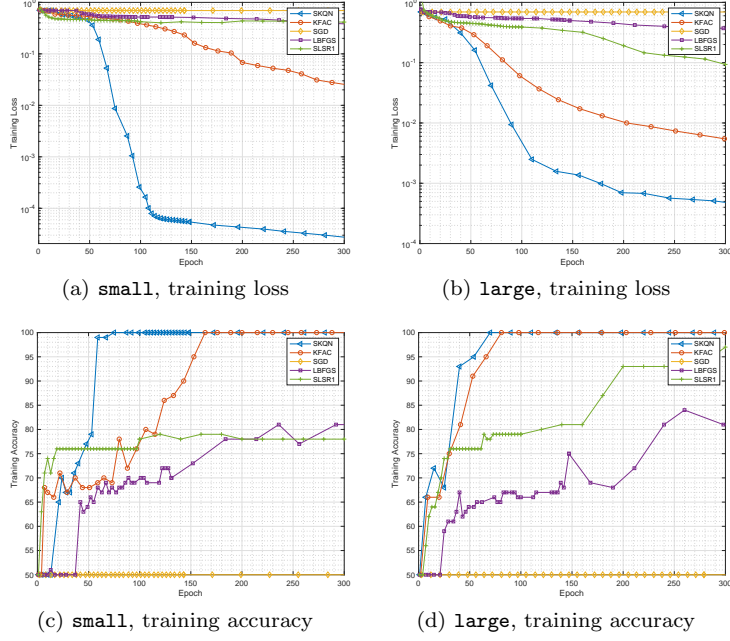


Figure 7: Toy neural network: Comparison of different algorithms on small and large network architectures.

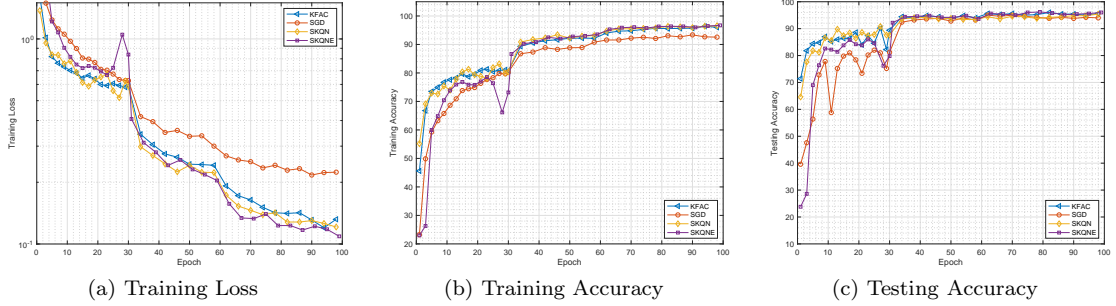


Figure 8: Deep CNN: Comparison of different algorithms on ImageNette.

Taking the expectation related to \mathcal{S}_g^k of (27) on both sides conditioned on \mathcal{F}_{k-1} and combining (27), (28) and (29), we obtain

$$\begin{aligned}
& \mathbb{E}[\Psi(\theta^{k+1}) - \Psi(\theta^k) | \mathcal{F}_{k-1}] \\
& \leq \left[4\left(\frac{\beta_k^2}{2\tau_k} + L_\Psi \beta_k^2\right) + \frac{\tau_k}{2} + \left(\frac{\beta_k^2}{2\tau_k} + L_\Psi \beta_k^2\right) 4L_\Psi^2 \alpha_k^2 h_2^2 + L_\Psi \alpha_k^2 h_2^2 - \alpha_k h_1 \right] \|\nabla \Psi(\theta^k)\|^2 \\
& \quad + \left(\frac{\beta_k^2}{\tau_k} + 2L_\Psi \beta_k^2\right) \cdot \sigma_{k,+}^2 + \left(\left(\frac{\beta_k^2}{2\tau_k} + L_\Psi \beta_k^2\right) 4L_\Psi^2 \alpha_k^2 h_2^2 + L_\Psi \alpha_k^2 h_2^2\right) \cdot \sigma_k^2.
\end{aligned} \tag{30}$$

Let $\tau_k = 2\beta_k$. Then, under the condition in Theorem 3 for the step sizes, we have

$$\begin{aligned}
& \frac{\tau_k}{2} + \left(\frac{\beta_k^2}{2\tau_k} + L_\Psi \beta_k^2\right) (4L_\Psi^2 \alpha_k^2 h_2^2 + 4) + L_\Psi \alpha_k^2 h_2^2 \\
& = 2\beta_k + 4L_\Psi \beta_k^2 + L_\Psi^2 \alpha_k^2 h_2^2 \beta_k + 4L_\Psi^3 \alpha_k^2 h_2^2 \beta_k^2 + L_\Psi \alpha_k^2 h_2^2 \\
& \leq 3\beta_k + \frac{3h_1}{8} \alpha_k \leq \frac{3}{4} h_1 \alpha_k.
\end{aligned}$$

Combining the relationship in (30), it holds almost surely that

$$\mathbb{E}[\Psi(\theta^{k+1}) - \Psi(\theta^k) | \mathcal{F}_{k-1}] \leq -\frac{1}{4}h_1\alpha_k\|\nabla\Psi(\theta^k)\|^2 + \beta_k\sigma_{k,+}^2 + \frac{3h_1}{8}\alpha_k\sigma_k^2. \quad (31)$$

Taking expectation, summing over the inequality and using the assumptions that there exists Ψ^* such that $\Psi(\theta) \geq \Psi^*, \forall \theta \in \text{dom}\Psi$, we obtain:

$$\sum_{k=1}^{\infty} \frac{1}{4}h_1\alpha_k\mathbb{E}\|\nabla\Psi(\theta^k)\|^2 \leq \Psi(\theta^1) - \Psi^* + \sum_{k=1}^{\infty} \beta_k\sigma_k^2 + \sum_{k=1}^{\infty} \frac{3h_1}{8}\alpha_k\sigma_k^2. \quad (32)$$

Therefore, we have $\sum_{k=1}^{\infty} \alpha_k\mathbb{E}\|\nabla\Psi(\theta^k)\|^2 < \infty$, which implies that $\sum_{k=1}^{\infty} \alpha_k\|\nabla\Psi(\theta^k)\|^2 < \infty$ almost surely. Consequently, we can infer

$$\liminf_{k \rightarrow \infty} \mathbb{E}\|\nabla\Psi(\theta^k)\|^2 = 0 \text{ and } \liminf_{k \rightarrow \infty} \nabla\Psi(\theta^k) = 0 \text{ almost surely.}$$

Taking expectation, multiplying α_k on both sides of inequality (29) and summing over all k yields

$$\sum_{k=1}^{\infty} \alpha_k\mathbb{E}\|\nabla_{S_g^k}\Psi(\theta^k)\|^2 \leq \sum_{k=1}^{\infty} \alpha_k\sigma_k^2 + \sum_{k=1}^{\infty} \alpha_k\|\nabla\Psi(\theta^k)\|^2 < \infty.$$

Applying the same way on (28) gives

$$\sum_{k=1}^{\infty} \alpha_k\mathbb{E}\|\nabla_{S_g^k}\Psi(z^k)\|^2 \leq 2\sum_{k=1}^{\infty} \alpha_k\sigma_{k,+}^2 + 4L_{\Psi}^2\alpha_k^2h_2^2\sum_{k=1}^{\infty} \alpha_k\mathbb{E}\|\nabla_{S_g^k}\Psi(\theta^k)\|^2 + 4\sum_{k=1}^{\infty} \alpha_k\mathbb{E}\|\nabla\Psi(\theta^k)\|^2 < \infty.$$

By the Young inequality, it implies

$$\begin{aligned} \sum_{k=1}^{\infty} \alpha_k^{-1}\mathbb{E}\|\theta^{k+1} - \theta^k\|^2 &= \sum_{k=1}^{\infty} \alpha_k^{-1}\mathbb{E}\|\alpha_k(B_k + \lambda_k I)^{-1}\nabla_{S_g^k}\Psi(\theta^k) + \beta_k\nabla_{S_g^k}\Psi(z^k)\|^2 \\ &\leq \sum_{k=1}^{\infty} 2\alpha_k h_2^2\mathbb{E}\|\nabla_{S_g^k}\Psi(\theta^k)\|^2 + \sum_{k=1}^{\infty} 2\alpha_k^{-1}\beta_k^2\mathbb{E}\|\nabla_{S_g^k}\Psi(z^k)\|^2 \\ &\leq \sum_{k=1}^{\infty} 2\alpha_k h_2^2\mathbb{E}\|\nabla_{S_g^k}\Psi(\theta^k)\|^2 + \sum_{k=1}^{\infty} \frac{\alpha_k}{8}\mathbb{E}\|\nabla_{S_g^k}\Psi(z^k)\|^2 \\ &< \infty. \end{aligned}$$

It follows that

$$\sum_{k=1}^{\infty} \alpha_k^{-1}\mathbb{E}\|\theta^{k+1} - \theta^k\|^2 < \infty \text{ and } \sum_{k=1}^{\infty} \alpha_k^{-1}\|\theta^{k+1} - \theta^k\|^2 < \infty \text{ almost surely.}$$

On the events $\mathcal{E} = \{\|\nabla\Psi(\theta^k)\| \text{ does not converge}\}$, there exists $\epsilon > 0$ and two increasing sequences $\{p_i\}_i, \{q_i\}_i$ such that $p_i < q_i$ and

$$\|\nabla\Psi(\theta^{p_i})\| \geq 2\epsilon, \quad \|\nabla\Psi(\theta^{q_i})\| < \epsilon, \quad \|\nabla\Psi(\theta^k)\| \geq \epsilon,$$

for $k = p_i + 1, \dots, q_i - 1$. Thus, it follows that

$$\epsilon^2 \sum_{i=0}^{\infty} \sum_{k=p_i}^{q_i-1} \alpha_k \leq \sum_{i=0}^{\infty} \sum_{k=p_i}^{q_i-1} \alpha_k \|\nabla\Psi(\theta^k)\|^2 \leq \sum_{k=0}^{\infty} \alpha_k \|\nabla\Psi(\theta^k)\|^2 < \infty. \quad (33)$$

Setting $\zeta_i = \sum_{k=p_i}^{q_i-1} \alpha_k$, it follows $\zeta_i \rightarrow 0$. Then by the Hölder's inequality, we obtain

$$\|\theta^{p_i} - \theta^{q_i}\| \leq \sqrt{\zeta_i} \left[\sum_{k=p_i}^{q_i-1} \alpha_k^{-1} \|\theta^{k+1} - \theta^k\|^2 \right]^{1/2} \rightarrow 0.$$

Due to the Lipschitz property of $\nabla\Psi$, we have $\|\nabla\Psi(\theta^{p_i}) - \nabla\Psi(\theta^{q_i})\| \rightarrow 0$, which is a contradiction. This implies $\mathbb{P}(\mathcal{E}) = 0$. Hence $\nabla\Psi(\theta^k)$ converges to zero almost surely.

In a similar fashion, we can also prove the convergence in expectation. Suppose that $\mathbb{E}\|\nabla\Psi(\theta^k)\|$ does not converge. There exists $\epsilon > 0$ and two increasing sequences $(p_i)_i, (q_i)_i$ such that $p_i < q_i$ and

$$\mathbb{E}\|\nabla\Psi(\theta^{p_i})\| \geq 2\epsilon, \quad \mathbb{E}\|\nabla\Psi(\theta^{q_i})\| < \epsilon, \quad \mathbb{E}\|\nabla\Psi(\theta^k)\| \geq \epsilon,$$

for $k = p_i + 1, \dots, q_i - 1$. Thus, it follows that

$$\epsilon^2 \sum_{i=0}^{\infty} \sum_{k=p_i}^{q_i-1} \alpha_k \leq \sum_{i=0}^{\infty} \sum_{k=p_i}^{q_i-1} \alpha_k \mathbb{E}\|\nabla\Psi(\theta^k)\|^2 \leq \sum_{k=0}^{\infty} \alpha_k \mathbb{E}\|\nabla\Psi(\theta^k)\|^2 < \infty. \quad (34)$$

Setting $\zeta_i = \sum_{k=p_i}^{q_i-1} \alpha_k$, it follows $\zeta_i \rightarrow 0$. Then by the Hölder's inequality, we have

$$\|\theta^{p_i} - \theta^{q_i}\| \leq \sqrt{\zeta_i} \left[\sum_{k=p_i}^{q_i-1} \alpha_k^{-1} \|\theta^{k+1} - \theta^k\|^2 \right]^{1/2} \rightarrow 0 \text{ almost surely.}$$

Due to the Lipschitz property of $\nabla\Psi$, we have $\mathbb{E}\|\nabla\Psi(\theta^{p_i}) - \nabla\Psi(\theta^{q_i})\| \rightarrow 0$, which is a contradiction. It implies that $\mathbb{E}\|\nabla\Psi(\theta^k)\|$ converges to zero. \square

D. Proof of Theorem 4

Proof. Taking expectation on both sides of the inequality (31), we obtain

$$\mathbb{E}[\Psi(\theta^{k+1}) - \Psi(\theta^k)] \leq -\frac{1}{4}h_1\alpha_k\mathbb{E}\|\nabla\Psi(\theta^k)\|^2 + \beta_k\sigma_{k,+}^2 + \frac{3h_1}{8}\alpha_k\sigma_k^2. \quad (35)$$

Summing the inequalities over $k = 1, 2, \dots, l-1$ yields

$$\begin{aligned} \mathbb{E}[\Psi(\theta^l) - \Psi(\theta^1)] &\leq -\frac{1}{4}h_1 \sum_{k=1}^{l-1} \alpha_k \mathbb{E}\|\nabla\Psi(\theta^k)\|^2 + \sum_{k=1}^{l-1} \beta_k \sigma_{k,+}^2 + \frac{3h_1}{8} \sum_{k=1}^{l-1} \alpha_k \sigma_k^2 \\ &\leq \sum_{k=1}^{\infty} \beta_k \sigma_{k,+}^2 + \frac{3h_1}{8} \sum_{k=1}^{\infty} \alpha_k \sigma_k^2. \end{aligned}$$

Hence, there is a constant M_Ψ such that $\mathbb{E}[\Psi(\theta^l)] \leq M_\Psi$ for any l . Dividing α_k on both sides of (35) and summing $k = 1, 2, \dots, l-1$, we obtain

$$\begin{aligned} \frac{1}{4}h_1 \sum_{k=1}^l \mathbb{E}\|\nabla\Psi(\theta^k)\|^2 &\leq \sum_{k=1}^l \frac{1}{\alpha_k} \mathbb{E}[\Psi(\theta^k) - \Psi(\theta^{k+1})] + \sum_{k=1}^l \frac{\beta_k}{\alpha_k} \sigma_{k,+}^2 + \frac{3h_1}{8} \sum_{k=1}^l \sigma_k^2 \\ &\leq \frac{1}{\alpha_1} \mathbb{E}[\Psi(\theta^1)] + \sum_{k=2}^l \left(\frac{1}{\alpha_k} - \frac{1}{\alpha_{k-1}} \right) \mathbb{E}[\Psi(\theta^k)] - \frac{1}{\alpha_l} \mathbb{E}[\Psi(\theta^{l+1})] \\ &\quad + \sum_{k=1}^l \frac{\beta_k}{\alpha_k} \sigma_{k,+}^2 + \frac{3h_1}{8} \sum_{k=1}^l \sigma_k^2 \\ &\leq \frac{M_\Psi}{\alpha_1} + M_\Psi \sum_{k=2}^l \left(\frac{1}{\alpha_k} - \frac{1}{\alpha_{k-1}} \right) - \frac{\Psi^*}{\alpha_l} + \left(\frac{1}{4} + \frac{3h_1}{8} \right) c \sum_{k=1}^l k^{-\chi} \\ &\leq \frac{M_\Psi - \Psi^*}{\varsigma} l^\nu + \left(\frac{1}{4} + \frac{3h_1}{8} \right) c \sum_{k=1}^l k^{-\chi} \\ &\leq \frac{M_\Psi - \Psi^*}{\varsigma} l^\nu + \left(\frac{1}{4} + \frac{3h_1}{8} \right) \frac{c}{1-\chi} (k^{1-\chi} - 1), \end{aligned}$$

which implies

$$\frac{1}{l} \sum_{k=1}^l \mathbb{E} \|\nabla \Psi(\theta^k)\|^2 \leq \frac{4(M_{\Psi} - \Psi^*)}{h_1 \varsigma} l^{v-1} + \left(\frac{1}{h_1} + \frac{3}{2}\right) \frac{c}{1-\chi} (l^{-\chi} - l^{-1}).$$

In order to ensure the inequality

$$0 \leq \frac{4(M_{\Psi} - \Psi^*)}{h_1 \varsigma} l^{v-1} + \left(\frac{1}{h_1} + \frac{3}{2}\right) \frac{c}{1-\chi} (l^{-\chi} - l^{-1}) \leq \epsilon \leq 1,$$

it is sufficient enough to require that the number of iterations l is at most $\mathcal{O}(\epsilon^{-\frac{1}{1-v}})$. \square

E. Proof of Theorem 6

Proof. For simplicity of notations, we set

$$\begin{aligned} w_1^k &= (A_k + H_k - \nabla^2 \Psi(\theta^*)) (\theta^{k+1} - \theta^k), \\ w_2^k &= \nabla \Psi(\theta^{k+1}) - \nabla \Psi(\theta^k) - \nabla^2 \Psi(\theta^*) (\theta^{k+1} - \theta^k). \end{aligned}$$

Then by the quasi-Newton scheme, we have

$$B_k(\theta^{k+1} - \theta^k) - \nabla^2 \Psi(\theta^*) (\theta^{k+1} - \theta^k) = -\nabla_{\mathcal{S}_g^k} \Psi(\theta^k) - \nabla^2 \Psi(\theta^*) (\theta^{k+1} - \theta^k).$$

It follows that

$$w_1^k - w_2^k = -\nabla \Psi(\theta^{k+1}) + \nabla \Psi(\theta^k) - \nabla_{\mathcal{S}_g^k} \Psi(\theta^k).$$

Due to Assumptions B.1-B.3, we have that $\|w_1^k\|/\|\theta^{k+1} - \theta^k\|$ and $\|w_2^k\|/\|\theta^{k+1} - \theta^k\|$ converges to 0 almost surely. It follows that

$$m_k := \frac{\|-\nabla \Psi(\theta^{k+1}) + \nabla \Psi(\theta^k) - \nabla_{\mathcal{S}_g^k} \Psi(\theta^k)\|}{\|\theta^{k+1} - \theta^k\|} \rightarrow 0 \text{ almost surely.}$$

By the nonsingularity of $\nabla^2 \Psi(x^*)$ and the convergence of $\{\theta^k\}$, with probability 1, there exists a constant ξ such that

$$\|\nabla \Psi(\theta^{k+1})\| \geq \xi \|\theta^{k+1} - \theta^*\|.$$

It implies that

$$\begin{aligned} m_k &\geq \frac{\|\nabla \Psi(\theta^{k+1})\| - \|\nabla \Psi(\theta^k) - \nabla_{\mathcal{S}_g^k} \Psi(\theta^k)\|}{\|\theta^{k+1} - \theta^*\| + \|\theta^k - \theta^*\|} \\ &\geq \frac{\xi \|\theta^{k+1} - \theta^*\| - \|\nabla \Psi(\theta^k) - \nabla_{\mathcal{S}_g^k} \Psi(\theta^k)\|}{\|\theta^{k+1} - \theta^*\| + \|\theta^k - \theta^*\|}. \end{aligned}$$

Define the events

$$\Gamma_k = \{\|\nabla_{\mathcal{S}_g^k} \Psi(\theta^k) - \nabla \Psi(\theta^k)\| \leq (c\eta_k^k)^{\frac{1}{2}}\}.$$

Then by the Chebyshev inequality, we obtain

$$\mathbb{P}(\Gamma_k | \mathcal{F}_{k-1}) \geq 1 - \frac{\sigma_k^2}{c\eta_k^k} \geq 1 - p_k.$$

It implies that $\sum_{k=1}^{\infty} \mathbb{P}(\Gamma_k^c) \leq \sum_{k=1}^{\infty} p_k < \infty$. By the Borel-Cantelli lemma, we have

$$\mathbb{P}(\cup_{k=1}^{\infty} \Gamma_k) = 1.$$

On the event $\cup_{k=1}^{\infty} \cap_{j=k}^{\infty} \Gamma_j$, there is a sufficiently large l_0 such that for any $k \geq l_0$, we have $m_k < \xi/2$ and $\|\nabla_{\mathcal{S}_j^k} \Psi(\theta^k) - \nabla \Psi(\theta^k)\| \leq (c\eta_k^k)^{\frac{1}{2}}$. Therefore, it follows that

$$\begin{aligned} \|\theta^{k+1} - \theta^*\| &\leq \frac{m_k}{\xi - m_k} \|\theta^k - \theta^*\| + \frac{(c\eta_k^k)^{\frac{1}{2}}}{\xi - m_k} \\ &\leq \frac{2m_k}{\xi} \|\theta^k - \theta^*\| + \frac{2(c\eta_k^k)^{\frac{1}{2}}}{\xi}. \end{aligned}$$

Set

$$\begin{aligned} \psi_{k+1} &= \max \left\{ \left(\frac{2}{\xi} m_k + \left(\frac{2(c\eta_k^k)^{\frac{1}{2}}}{\xi} \right)^{\frac{1}{2}} \right) \psi_k, \left(\frac{2(c\eta_{k+1}^{k+1})^{\frac{1}{2}}}{\xi} \right)^{\frac{1}{2}} \right\}, \\ \psi_{l_0} &= \max \left\{ \|\theta^{l_0} - \theta^*\|, \left(\frac{2(c\eta_{l_0}^{l_0})^{\frac{1}{2}}}{\xi} \right)^{\frac{1}{2}} \right\}. \end{aligned}$$

By induction and the fact that $\psi_k \geq \left(\frac{2(c\eta_k^k)^{\frac{1}{2}}}{\xi} \right)^{\frac{1}{2}}$, we obtain that for any $k \geq l_0$,

$$\|\theta^{k+1} - \theta^*\| \leq \frac{2m_k}{\xi} \psi_k + \left(\frac{2(c\eta_k^k)^{\frac{1}{2}}}{\xi} \right)^{\frac{1}{2}} \psi_k \leq \psi_{k+1}.$$

Finally, we show that ψ_k has a superlinear convergence rate. Since m_k, η_k converge to 0 and $\eta_{k+1} \leq \eta_k$, the sequence ψ_k converges to 0 and

$$\frac{\psi_{k+1}}{\psi_k} \leq \max \left\{ \left(\frac{2}{\xi} m_k + \left(\frac{2(c\eta_k^k)^{\frac{1}{2}}}{\xi} \right)^{\frac{1}{2}} \right), \frac{(\eta_{k+1}^{k+1})^{\frac{1}{4}}}{(\eta_k^k)^{\frac{1}{4}}} \right\} \rightarrow 0,$$

which completes the proof. □

F. Proof of Proposition 8

Proof. Define the events

$$\begin{aligned} \Xi_k &= \{ \|\mathbf{N}(\nabla_{\mathcal{S}_H^k}^2 \Psi(\theta^k)) - \nabla_{\mathcal{S}_H^k}^2 \Psi(\theta^k)\|_1 \geq \gamma_k \}, \\ \Upsilon_k &= \{ \|\nabla_{\mathcal{S}_H^k}^2 \Psi(\theta^k) - \nabla^2 \Psi(\theta^k)\| \geq \sqrt{\gamma_k} \}. \end{aligned}$$

Then by the Chebyshev inequality and Theorem 1, we obtain

$$\begin{aligned} \mathbb{P}(\Xi_k | \mathcal{F}_{k-1}) &\leq \frac{(n+1) \|\nabla_{\mathcal{S}_H^k}^2 \Psi(\theta^k) - [\nabla_{\mathcal{S}_H^k}^2 \Psi(\theta^k)]_{s_k}\|_1}{\gamma_k} \leq (n+1)p_k, \\ \mathbb{P}(\Upsilon_k | \mathcal{F}_{k-1}) &\leq \frac{\omega_k^2}{\gamma_k} \leq p_k. \end{aligned}$$

It implies that $\sum_{k=1}^{\infty} \mathbb{P}(\Xi_k) \leq \sum_{k=1}^{\infty} (n+1)p_k < \infty$ and $\sum_{k=1}^{\infty} \mathbb{P}(\Upsilon_k) \leq \sum_{k=1}^{\infty} p_k < \infty$. By the Borel-Cantelli lemma, we have

$$\mathbb{P}(\cup_{k=1}^{\infty} \cap_{j=k}^{\infty} \Xi_j^c) = 1, \quad \mathbb{P}(\cup_{k=1}^{\infty} \cap_{j=k}^{\infty} \Upsilon_j^c) = 1,$$

which implies that $\|\nabla_{S_H^k}^2 \Psi(\theta^k) - \nabla^2 \Psi(\theta^k)\|$ and $\|\mathbf{N}(\nabla_{S_H^k}^2 \Psi(\theta^k)) - \nabla_{S_H^k}^2 \Psi(\theta^k)\|_1$ converge to 0 almost surely. Hence, it holds almost surely that

$$\lim_{k \rightarrow \infty} \frac{\|(\nabla_{S_H^k}^2 \Psi(\theta^k) - \nabla^2 \Psi(\theta^k))(\theta^{k+1} - \theta^k)\|}{\|\theta^{k+1} - \theta^k\|} = 0 \text{ and } \lim_{k \rightarrow \infty} \frac{\|(\mathbf{N}(\nabla_{S_H^k}^2 \Psi(\theta^k)) - \nabla_{S_H^k}^2 \Psi(\theta^k))(\theta^{k+1} - \theta^k)\|}{\|\theta^{k+1} - \theta^k\|} = 0.$$

Consequently, a simple calculation shows that Assumption B.3 holds.

□